Optimization and Design of a Cascaded DC/DC Converter Devoted to Grid-Connected Photovoltaic Systems

Stéphane Vighetti, Jean-Paul Ferrieux, and Yves Lembeye

***Abstract*—The integration of photovoltaic (PV) modules in buildings causes problems with shadows that can strongly reduce the energy produced by these systems. Moreover, most PV modules are designed for stand-alone applications that have output voltage adapted to lead batteries. Indeed, this historical sizing of PV modules can be discussed in the case of grid-connected systems. In this paper, a cascaded dc/dc converter based on boost chopper is proposed. First, the advantages and the limits of this topology will be shown. Second, this topology will be optimized to maximize the efficiency or minimize the volume. The originality of this optimization is that the converters' parameters and the arrangement of the PV cells are variable parameters. Indeed, the optimization is done on the entire system. To realize these optimizations, semiempiric models of losses and volumes of different components of a boost chopper were developed. The optimization uses a successive quadratic programming algorithm. Considering the optimization results over the whole range of the specifications, a flexible solution is developed and experimental results are presented. Finally, optimized topologies connected to several PV are evaluated at different situations of typical shadows.**

***Index Terms*—DC/DC converter, optimization, photovoltaic, power electronics, shade.**

NOMENCLATURE

PV	Photovoltaic.
MPPT	Maximum power point tracking.
V_{ei}, I_{ei}, and P_{ei}	Input voltage, input current, and input power.
V_s, I_s, and P_s	Output voltage, output current, and output power.
α_i	Duty cycle.
n	Number of PV cells per converter.
n_{tot}	Total number of cells.
m	Number of converters.
F	Switching frequency.
ΔI	Input current ripple.
L	Input inductance of a boost converter.
R_{dson}	Static drain-source on state resistance of MOSFET.
C_{oss}	Output capacitance of MOSFET.
I_{RM}	Maximum reverse recovery current.
C_d	Capacitance of diode.
Q_{RR}	Reverse recovery charge.
V_F	Forward voltage.
η	Efficiency.
Irr	Irradiation.

Manuscript received January 25, 2011; revised May 3, 2011; accepted July 16, 2011. Date of current version February 20, 2012. Recommended for publication by Associate Editor K. Ngo.

The authors are with the Grenoble Electrical Engineering Laboratory (G2Elab), UMR 5269 (Grenoble-INP/UJF, CNRS), 38402 Saint Martin d'Hères Cedex, France (e-mail: stephane.vighetti@hotmail.fr; Jean-Paul.Ferrieux@g2elab.grenoble-inp.fr; Yves.Lembeye@g2elab.grenoble-inp.fr).

Color versions of one or more of the figures in this paper are available online at http://ieeexplore.ieee.org.

Digital Object Identifier 10.1109/TPEL.2011.2167159

I. INTRODUCTION

THIS study deals with the optimization of the conversion line for a grid-connected PV. Grid-connected applications have experienced strong development over the past few years, thanks to the very attractive price incentives of the electricity produced by this kind of application [1], [2]. This study is aimed at residential PV installations. The typical power of this system is included between 1 and 5 kWp. It is assumed that the PV technology used is a crystalline one, because of its large spreading on the current market [3]. These devices, with their strong building integration and their development in urban zones can be subjected to severe shadows. Under these conditions, the PV field works under mismatching conditions that can lead to important power losses [4], [5]. The proposed solution will have to decrease the effects of shadow and keep the reliability and the cost imposed by the market [6]–[9]. This work focuses on the choice of different stages of conversion and the arrangement of the PV cells. The topology, the sizing, and the technology of different stages of conversion will be determined to define the optimum topology based on the characteristics of the PV cells.

II. STUDIED PV FIELD TOPOLOGY

The state of the art has revealed numerous advantages of cascaded dc/dc converters between PV modules and the inverter to reduce the impact of shadow and maximize the produced energy [10]. The boost converter has become of great interest in this field topology. Indeed, its voltage rising, its high efficiency, its reliability, the possibility of implementing a MPPT, and its low price are decisive advantages [11], [12]. Thus, numerous interests can be brought by this field topology (see Fig. 1). This topology will be studied in this paper.

Moreover, the historical stand-alone applications have led to a PV module's output adapted to the lead battery (12 or 24 V). This sizing can be discussed for grid-connected applications; however, few papers reconsider it. Nowadays,

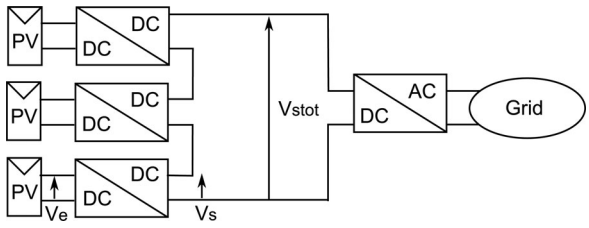

Fig. 1. Studied PV field topology.

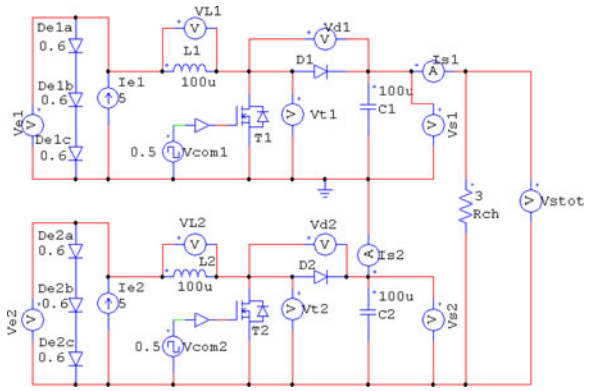

Fig. 2. PSIM simulations scheme.

power electronics is optimized with industrial PV modules. This work develops two main originalities:

1) the optimization is made on the entire system;
2) the historical PV sizing is reconsidered.

The dc/ac stage is not studied here but further information can be found in [13]–[15] and [34]–[36].

III. Validation of the Topology Used

Some simulations have been carried out to check the correct operating of the topology introduced in Fig. 1.

The following hypotheses have been made in these simulations:

1) two cascaded boost converters;
2) three PV cells per converter;
3) components are ideal;
4) the resistance R_{ch} (see Fig. 2) simulates an inverter connected to the grid. The adaptation of its value allows us to extract the whole power;
5) PV cells have a voltage of 0.6 V and a current of 5 A under standard test conditions (STC);
6) the nominal duty cycle α of converters is 0.5;
7) each boost operates in continuous conduction mode.

The simulation scheme is shown in Fig. 2. The different parameters and results are presented in Table I.

The first simulation checks the nominal operating point (simulation 1). All PV cells have the same operating point and the topology is able to extract the entire available power of each PV cell.

Moreover, these simulations can be of interest to this topology in the case of shadow. Indeed, simulation 2 illustrates a case where two PV generators have two different working points and

TABLE I
Parameters and Results of Simulation Realized With PSIM

	Simulation 1	Simulation 2	Simulation 3
Ve1	1.8 V	1.5 V	1.5 V
Ie1	5 A	2.5 A	1 A
Pe1	9 W	3.75 W	1.5 W
α1	0.5	0.646	0
Ve2	1.8 V	1.8 V	1.8 V
Ie2	5 A	5 A	5 A
Pe2	9 W	9 W	9 W
α2	0.5	0.292	0.75
Vs	7.2 V	7.2 V	7.2 V
Is	2.5 A	1.77 A	1.25 A
Ps	18 W	12.75 W	9 W

shows that this topology is able to balance currents. Every boost can supply the whole input power to the output, and is also able to regulate the output voltage at the desired value [12]. In this simulation, duty cycles are recalculated in order to obtain the same output voltage for unbalanced cases. For real cases, duty cycles will be tuned by using an individual MPPT.

To study this system, it can be noted that the output current in a series string of converters must be equal, and the constraints for boost converters are $V_{\mathrm{in}} \leq V_{\mathrm{out}}$ and $I_{\mathrm{in}} \geq I_{\mathrm{out}}$. A limit can appear when one PV generator is shaded; its current will fall. If this value is lower than the string output current, the string output current must be set to the value of the shaded cell current. In order to avoid this state, the topology is able to shunt the weak PV generator, thanks to the reverse diode of the MOSFET (simulation 3). In this case, all other cells can normally work and continue to provide the maximum of their energy. The weak cell(s) is (are) then shunted.

Simulations have been carried out using PSIM software. They confirm that the topology can work in any rate of conditions, which is of real interest in the case of shadow.

IV. Topology Optimization

This study aims to adapt the PV modules and the converters for a grid-connected application. An optimization of the efficiency or the volume of the topology introduced in Fig. 1 has been accomplished. The goal of this optimization is to find the "n" and "m" pair to maximize produced energy. The number "n" is the number of cells to connect in series on the input of each boost and "m" is the number of boosts to cascade. This optimization must also define the optimum working point of the boost (frequency, input ripple current, and input voltage). Fig. 3 shows the topology to optimize.

The maximum number of cells is set in the first optimization to 144, which represents the number of cells of two current PV modules. This restriction limits the voltage ratio of the converters to 5 in order to decrease losses in the boost. A 5-in-multicrystalline cell has been used to realize this work (Photowatt, PW 1650, 165 W).

The field of definition of the different parameters is defined in Table II. These values are directly set by the characteristics of the topology and its working constraints.

Table II also defines the limits of the optimization and the validity of models of losses and volumes that are developed in

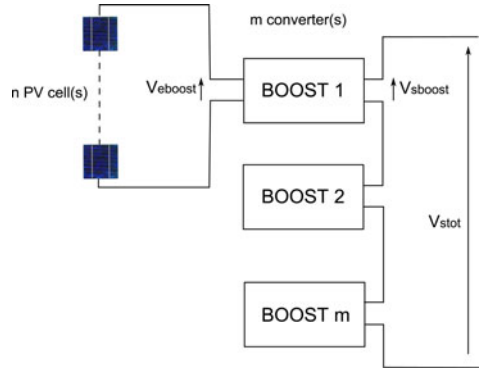

Fig. 3. Topology to optimize.

TABLE II
FIELD OF DEFINITION OF THE PARAMETERS

Parameter	Field of definition
n	1 < n < 144
m	1 < m < 144
n_{tot}	144
Frequency	20 kHz < F < 200 kHz
Input ripple current of boost	10 % < ΔI < 50 %
Input inductance of boost	0.9 µH < L < 6.5 mH
Semiconductor voltage rate	0 V < V < 400 V
Semiconductor current rate	5 A < I < 10 A
Cell current	5 A
Cell voltage	0.6 V
Duty cycle	0.76

the next part. The range of value of inductor "L" is calculated in continuous-conduction mode which represents the usual case of operating

$$L = \frac{\alpha V_{\text{in}}}{\Delta I\, F}. \tag{1}$$

Whatever the choice of the parameters "m" or "n," the duty cycle α has the same value (0.76) corresponding to the cell input voltage (0.6 V) and the output voltage (360 V). Consequently, the value of L is determined with relation (1) and the ranges of parameters are defined in Table II.

V. MODELS OF LOSSES AND VOLUMES

A. Models of Losses

Losses in a boost converter are due to four components: the inductance, the MOSFET, the diode, and the capacitor. It is assumed that capacitor losses are neglected considering its weak influence in front of other components.

Concerning the semiconductor, conduction losses, switching losses and also Miller effect losses were modeled with the classical model. The model of these losses is based on the following

TABLE III
MODELS OF THE VOLTAGE-DEPENDENT PARAMETERS

	Equations	
Losses in Mosfet	$R_{dson} = 1.51\times10^{-2}\times V_m - 0.1143$	(4)
	$C_{oss} = 5.33\times V_m^4 - 8.24\times10^{-18}\times V_m^3 + 4.11\times10^{-15}\times V_m^2 - 7.71\times10^{-13}\times V_m + 5.56\times10^{-11}$	(5)
Losses in Mosfet induced by diode	$I_{RM} = 5.6\times10^{-4}\times V_d^{1.59}$	(6)
	$C_d = 9.92\times10^{-10}\times V_d^{-.08}$	(7)
Losses in diode	$Q_{RR} = 1.30\times10^{-11}\times V_d^{1.42}$	(8)
	$V_F = 2.35\times10^{-3}\times V_d + 0.421$	(9)

equations:

$$\begin{aligned}\text{Losses}_{\text{MOS}} &= R_{\text{dson}}\times I_{\text{rms}}^2 + \frac{1}{2}\times V_m\times(I_{T\text{on}} + I_{\text{RM}})\\ &\quad\times(t_{\text{on}} + t_{\text{RM}})\times F + \frac{1}{2}\times I_{T\text{off}}\times t_{\text{off}}\times V_m\\ &\quad\times F + \frac{1}{2}\times(C_{\text{oss}} + C_d)\times V_m^2\times F \end{aligned}\tag{2}$$

$$\text{Losses}_D = V_F(I)\times I_{dmoy} + V_d\times Q_{\text{RR}}\times F. \tag{3}$$

An important work of modeling and normalization of the different parameters (R_{dson}, C_{oss}, C_d, Q_{RR}, I_{RM}, V_F) has also been carried out to express losses in semiconductors [16]. This work is based on different datasheets of various manufacturers. Some hypotheses have been proposed. The current slope at the turn-on of the MOS is defined at the average value of 200 A·μs^{-1} and t_{off} is fixed to 40 ns. V_F is studied for a current of 5 A. In this case, previous parameters only depend on the voltage rating of the semiconductor and can be normalized according to this parameter. Therefore, the evolution of each influent parameter on the losses of semiconductors is known according to the voltage of the semiconductor. The equations of the model are shown in Table III.

Concerning inductance losses, it has been necessary to precalculate them to obtain a table of values according to the frequency F, the ripple current ΔI, and also the inductance value L. Inductor design has been performed by using a MATLAB tool based on Dowell method for copper losses and Steinmetz approach for magnetizing losses [17]–[19]. To obtain the derivable function needed for the optimization process, these results have been linearized using Featuring General Optimisation Tool (FGOT) [20]. This linearization has given equation (3) that represents the evolution of losses according to the previously presented parameters

$$\begin{aligned}\text{Losses\_}L &= -2.77655435\times10^{-1} + 1040.912614\times L\\ &\quad + 3.136132503\times10^{-2}\times\Delta I + 13.4766738\\ &\quad\times\Delta I\times L - 4.25\times10^{-4}\times\Delta I^2 + 1.709015082\\ &\quad\times10^{-6}\times F + 1.283492743\times10^{-3}\times F\times L\\ &\quad - 5.0\times10^{-8}\times\Delta I\times L. \end{aligned}\tag{3}$$

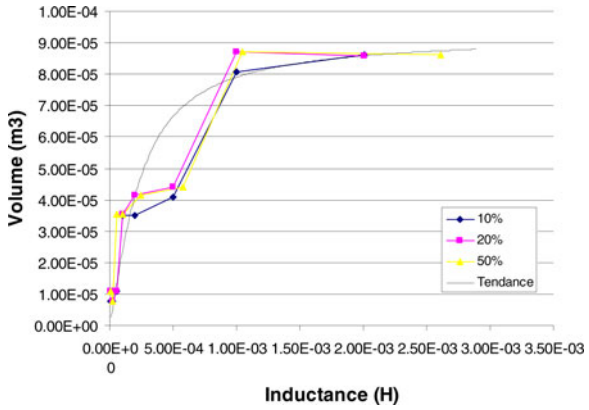

Fig. 4. Volume of inductor versus its value.

This equation is defined for the field of definition shown in Table II.

B. Models of Volume

The models of volume have been fitted by using some real cases sizing for heatsinks and inductors and by using datasheets for capacitors [16].

Basically, the volume of a semiconductor can be considered as the volume of the cooling system needed to refresh the chip. So, with datasheets of chips and heatsinks, an equation of the volume in function of needed thermal resistance has been defined

$$\text{Vol\_rad} = 5.68 \times 10^{-4} \times R_{\text{thrad}} - 1.48. \quad (4)$$

For the inductor, its volume is deduced from the design tool mentioned earlier and the results are shown in Fig. 4.

This volume depends on the dimensions of core and the number of turns and these dimensions are directly linked to the value of inductance (12). On the other hand, the switching frequency and current ripple have a negligible influence on this volume

$$\text{Vol\_}L = 5912 \times 10^{-5} \times \arctan(4.192 \times 10^{-3} \times L). \quad (5)$$

Finally, the volume of the capacitor has been studied by referring to the datasheet values of electrolytic capacitors and it has been shown that the volume of the capacitor evolves linearly according to the applied voltage

$$\text{Vol\_capa} = 1.17 \times 10^{-8} \times V_C + 3.13 \times 10^{-7}. \quad (6)$$

VI. Validation of the Losses Models

Before optimizing the topology, the model of losses presented in the previous section needs to be validated. So the results given by these models were compared to losses calculated by the design of two real converters. The results are presented in Table IV.

It can be noted that results obtained by the two methods are quite similar; the differences are less than 5%. The results of losses calculation in diodes and inductance are less accurate but their low values do not impact the global result. So, models can be considered as coherent and sufficiently accurate for the first optimization approach.

TABLE IV
Comparison of the Optimization and the Design Values

	1 converter (F = 20 kHz, ΔI = 50 % and L = 1.313 mH)		8 converters (F = 37 kHz, ΔI = 17 % and L = 225 µH)	
	Calculated values	Optimization values	Calculated values	Optimization values
Losses in Mosfet	21 W	23,1 W	38,8 W	38,1W
Losses in diodes	1,8 W	2,1 W	4,8 W	5,15 W
Losses in inductance	3,44 W	2,5 W	3,3 W	4,02 W
Total losses	26.2 W	27,7 W	46,9 W	47,2 W

TABLE V
Results of the Two Optimizations

Parameters	η European maximising optimization	Volume minimising optimization
m	2.02	9.63
n	71.3	14.96
F	31 511 Hz	122 302 Hz
ΔI	12 %	50 %
L	1 700 µH	223 µH
Volume	408 cm^3	235 cm^3
η_{euro}	94.8 %	87.1 %

VII. Optimizations Results Without Shadow

Two optimizations were accomplished: the first one for the minimization of the volume of the converter and, the second one, for the maximization of European efficiency. This European efficiency takes into account the variation of the solar resource during one day and one year. This efficiency can be viewed like an energetic efficiency. Its expression is $\eta_{\text{euro}} = 0.03 \times \eta_5 + 0.06 \times \eta_{10} + 0.13 \times \eta_{20} + 0.1 \times \eta_{30} + 0.48 \times \eta_{50} + 0.2 \times \eta_{100}$ (7) where η_x is the efficiency at $x\%$ of the typical power [21]. The different optimizations have been carried out with the software CADES [22]. For this work, a determinist algorithm has been used. The results are shown in Table V.

A. Maximization of the European Efficiency

In this optimization, all parameters are continuous, even if m and n are in reality two integer parameters. The solution given by the optimization is 2.02 converters. This solution is physically impossible. Nevertheless, this solution is very close to the topology with two converters. After checking, the difference of the parameters between both cases is negligible.

Fig. 5 shows that the efficiency is maximal for a topology with two converters and efficiency decreases as the number of converters increases.

The optimization of the European efficiency leads to a topology with two converters and 72 PV cells per converter. Each converter operates at 30 kHz frequency and the ripple input current ΔI is 12%. This optimization shows that the efficiency remains high (greater than 90%) while the number of converters is under 10.

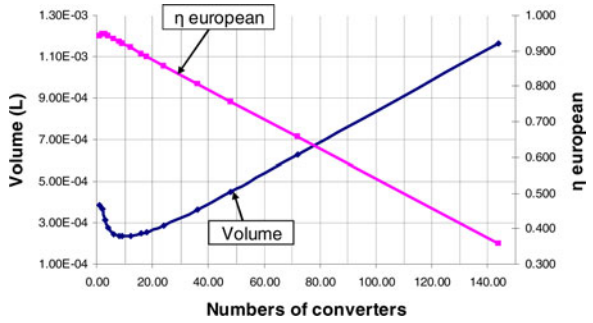

Fig. 5. Volume and European efficiency behavior versus number of converters.

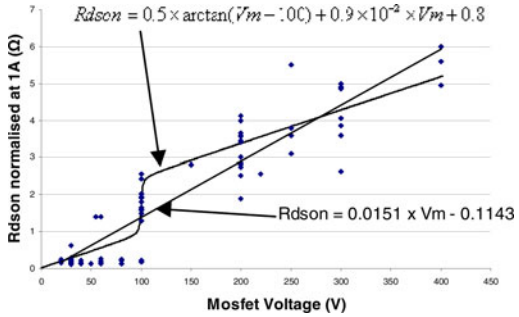

Fig. 6. $R_{\rm dson}$ versus MOS voltage.

TABLE VI
RESULTS OF THE OPTIMIZATION WITH $n_{\rm tot} = 288$

Parameters	η European maximising optimization
m	1.76
n	163
F	21.63 kHz
ΔI	10 %
L	3.1 mH
Volume	668 cm^3
η_{euro}	97.3 %

TABLE VII
CHARACTERISTICS OF THE OPTIMUM CONVERTERS FOR THE FOUR SCENARIOS

Optimisation	Number of converter	Nominal input voltage (V)	Nominal output voltage (V)
144 - linear	2.02 → 2	36	190
144 - arctan	4.13 → 4	18	95
288 - linear	1.76 →2	72	190
288 - arctan	3.90 → 4	36	95

B. Minimization of the Volume

The optimal solution when leading to a minimal volume is close to 10 converters. The frequency (122 kHz) and the input ripple current (50%) are much higher than the European efficiency optimization topology.

The minimum volume is 235 cm^3. This volume is two times less than the volume of the optimized efficiency topology. The efficiency of this optimized volume topology falls to 87.1%.

This volume optimization shows that volumes of the optimized efficiency topology remain reasonable compare to the optimal volume. Moreover, the volume is less restrictive than efficiency. The available volume on the back of the PV module is enough to insert many converters. Consequently, only the efficiency will be taken into account in the following study.

C. Sensitivity of the Optimization to the Specifications

To check the results obtained and to check the sensitivity of these results to the specifications and to the parameters of the models, some other optimizations have been done.

1) Sensitivity to the Specifications: First, the specifications have been modified. In this optimization, the total number of PV cells "$n_{\rm tot}$" is equal to 288. All the other parameters are kept constant. The results of this optimization with the new specification are shown in Table VI.

The efficiency of this structure is higher than in the first optimization. The input voltage is higher in this case, so the converter has a smaller voltage ratio (near to 2). The efficiency is logically better in this case.

For this optimization and for the optimization with 144 PV cells, the optimum is a structure with two converters. The input voltage has no influence on the optimum. The position of the optimum is determined by the output voltage of the converter. These converters are optimum for an output voltage of 180 V.

All the other parameters of the specifications have no impact on the results.

2) Sensitivity to the Parameters of the Models: Second, the sensitivity of the optimization to the parameters of the models has been checked and has shown that the optimization is not sensitive to the modification of the parameters of the models. Only one parameter has an impact on the results in function of its modeling. The repartition of $R_{\rm dson}$ in function of the MOSFET voltage is dispersed, so this parameter is difficult to linearize.

In this study, the linearization of $R_{\rm dson}$ is made with a linear function and with an "arctan" function (see Fig. 6). The results are different and the "arctan" approximation gives optimum structure with more converters.

The optimum structure depends on the specifications of the PV system and on the modeling of $R_{\rm dson}$. The different optimum structures are shown in Table VII.

A flexible technical solution able to adapt to different specifications is developed in the next section.

VIII. FLEXIBLE DC/DC CONVERTER

According to the optimization results from Table VII, a dc/dc converter has been realized in order to validate the result of the optimized topologies. The converter has been built in two different ways. One way is to maximize the efficiency and the second way is to have a flexible converter which can run with a wide range of input/output voltage and power. The concept of a flexible converter is presented in [23].

A. Flexible Converter

The converter has to be able to accept a wide range of powers and input/output voltage values. All this work permits a converter which could be used for several sizes of PV modules, so with several powers and voltage values. The converter can boost input voltage value from below 7 V up to 450 V and can run

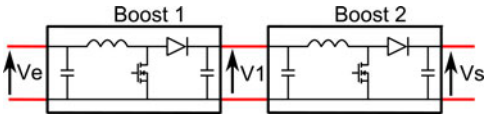

Fig. 7. Cascaded boost converter scheme.

TABLE VIII
CONFIGURATION OF THE CONVERTER VERSUS THE OPTIMIZATION RESULTS

Optimisation	Configuration of the converter
144 - linear	Cascaded Boost 1 and Boost2
144 - arcos	Boost 1
288 - linear	Boost 2
288 - arcos	Boost 1

from 6 to 500 W. In order to respond to this flexible function, the converter has been realized with two cascaded boosts as shown in Fig. 7 [10]. According to the input and output voltage values from the specifications, the converter makes possible the use of only a single boost or both.

Each boost has been built on the same architecture; the differences between the two boosts are the current and voltage constraints on components.

Connecting boosts in cascade with different ratings permits switching between several configurations according to the optimization shown in Table VIII.

B. Optimization of the Efficiency

The converter is built with the purpose of optimizing the efficiency without taking care of the volume. The only constraint imposed is the thickness which has to be lower than the aluminum frame of a PV module.

In order to maximize the efficiency, technologies used for semiconductors are CoolMos and SiC diode. CoolMos gives better performances than traditional MOSFET in the switching and on-state losses [24]. The lower forward voltage drop and switching losses of the SiC Schottky diodes provide a better efficiency than the conventional silicon diode [25]. The first stage is realized with 100 V voltage rate components (Vishay MOSFET SUP90N10-8m8P and Schottky diode16CTT100). The second one uses Infineon CoolMOS (IPP60R199CP) and SiC rectifier (SDT12S60).

The two inductors have been realized with the same planar core (GER 44*27*10) and Litz wire (20 turns for the first boost and 30 turns for the second boost, and 0.8 mm airgap for both).

The frequency, the current ripple, and the inductance value are chosen according to the European efficiency optimization results (see Table V).

A microcontroller is used to control the converter which has the characteristic of being small and having very low consumption.

C. Experimental Tests

An MPPT program has been implanted in the device. The MPPT algorithm is based on the Hill Climbing method [26]. This method is simple, gives an accurate tracking of the maximum power point, and can be easily programmed in a numerical control. Other new techniques of MPPT can improve the efficiency of the whole system [27]–[30], [37], [38].

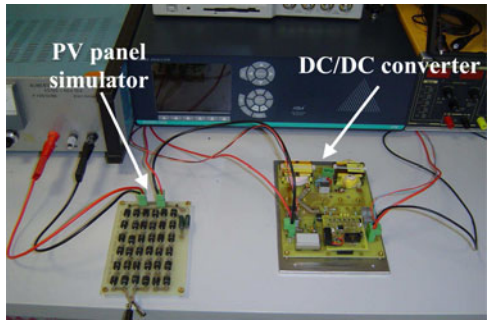

Fig. 8. DC/DC converter.

TABLE IX
TEST RESULTS

Optimisation	Maximal efficiency	European efficiency
144 - linear	96.80	95.78
144 - arctan	97.1	96.12
288 - linear	98.07	97.68
288 - arctan	98.10	97.26

Experimental test and measurement of the efficiency have been performed in order to compare to them simulation results. The results of this test are shown in Table IX.

Experimental results are coherent with the optimization results. The converter (see Fig. 8) is able to work in all specifications given by the optimizations and maintain good efficiency. This converter can be easily adapted to different PV field topology.

IX. INTEGRATION OF THE SHADOW EFFECTS

The optimizations and the test performed in the previous paragraphs do not take into account different shadow issues. When a PV cell is shaded, the power loss is proportional to the severity and surface of the shadow. Moreover, the shaded cell can impact all the cells connected in series [31]. If by-pass diodes are put in antiparallel, a shaded cell can be enough to shunt all cells linked to the same by-pass diode. The impact of the shaded cells on the energy produced may be very different according to their positions. In this study, the impact of the shadow on the energy production is realized on 144 PV cells using a linear model for R_{dson}; nevertheless, these results can be translated for other cases.

A. Influence of the Shadow Position

Both minimal and maximal shadow cases have been simulated. Indeed, shaded cells may all be located on the same group (concerned by the same by-pass diode); in this case, only this group is affected by the shadow. This case is called “grouped” and leads to minimal impact. The second case puts the shaded cells in different groups (in different by-pass diodes). In this

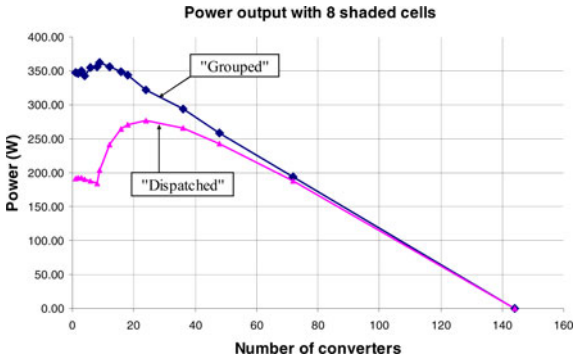

Fig. 9. Impact of eight shaded cells on the power versus the converters number.

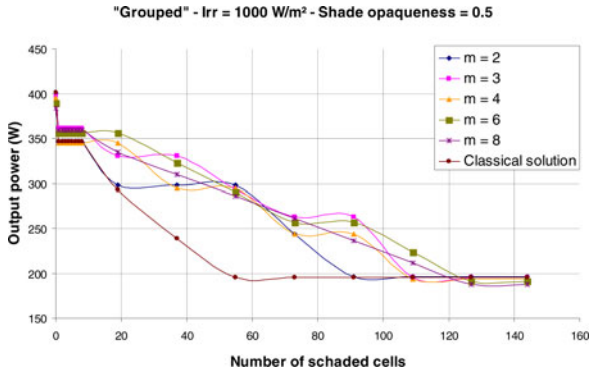

Fig. 10. Output power of different topologies versus the shaded cell number.

case, the shadow has a maximum impact on the output power. This case is called "dispatched."

The study of a particular case in which 8 of the 144 cells are shaded (see Fig. 9) has shown that the position of the shaded cells can divide the output power by nearly 2.

These results are strongly linked to the number and the position of shaded cells, and to the severity of the shadow.

B. Model of Shadow Effects

A program has been written to take into account the dependence of the previous results on the number of shaded cells, to their positions on the module, to the number of converters, and to the solar irradiance. The program is able to calculate the annual PV energy produced by a PV system on a roof in which a chimney is casting a shadow.

Inputs: The position of the module on the roof and the size of the chimney can be defined. The program uses the real solar resource of the considered geographical situation to calculate the position and the power of the sun. It uses the data given by the different optimizations to define the parameters of the converters used.

Outputs: The calculation of the power output is performed for every hour and is considered constant during this hour. The power output calculation takes into account the number of PV cells shaded, the solar power and its position, and the efficiency of the converter at this working point.

To obtain the energy produced during one year, the program calculates the integration of the output power. Some examples of results are studied in the following paragraphs.

C. Study at Constant Solar Irradiance

Before studying a real case, a study at constant solar irradiance has been done. In this test, the classical solution will be compared to topologies with two, three, four, six, and eight boosts for different cases of shadow. The output power will be the quantity compared to define the best topology in this case. Here, this test is made under STC and the shadow has an opaqueness of 50%. The study of the classical solution with only one converter ($m = 1$) takes into account the effect of by-pass diodes each 18 cells.

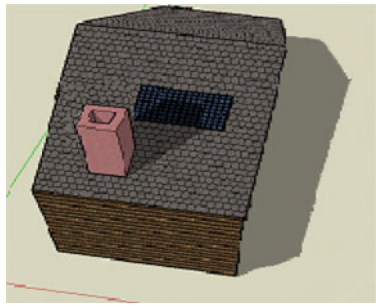

Fig. 11. Studied case.

The results of these comparisons presented in Fig. 10 highlight some conclusions.

The topologies proposed in this paper are more efficient than the classical solution when there are 20 to 90 shaded cells. The results are the same if the shaded PV cells are dispatched.

When there is no shade and all the fields are shaded, the topology with two boosts is the most competitive topology.

D. Effect of a Chimney

Previously, the shadow was modeled by a number of shaded cells and the impact has been estimated for a particular working point. In this part, to have a more realistic case and to take into account the daily and annual evolution of solar irradiance, the study will be done on a typical case.

The study will estimate the energy that different topologies can produce during one year with a typical shadow. The typical shadow chosen here is due to a chimney located on the southeast of the PV modules (see Fig. 11). The chimney shades between 2 and 28 PV cells from 2 P.M. to 4 P.M.. The solar data used here is based on Grenoble (southeast of France, 45° parallel) [32].

The classical solution is able to produce between 410 kWh (if the shaded PV cells are grouped) and 380 kWh (if the shaded PV cells are dispatched) (see Figs. 12 and 13). The PV installation has a typical power of 340 W.

The energy values obtained are coherent with the average values for the region of Grenoble, France (between 1100 and 1200 Wh/Wp installed) [32]. This remark confirms the validity and the accuracy of the models and MATLAB program.

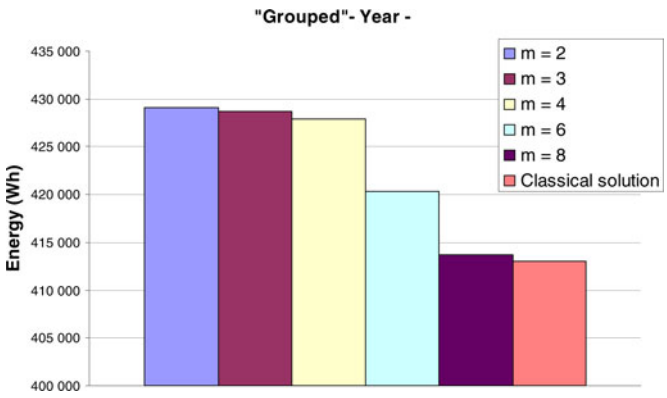

Fig. 12. Yearly energy produced (grouped shaded cells).

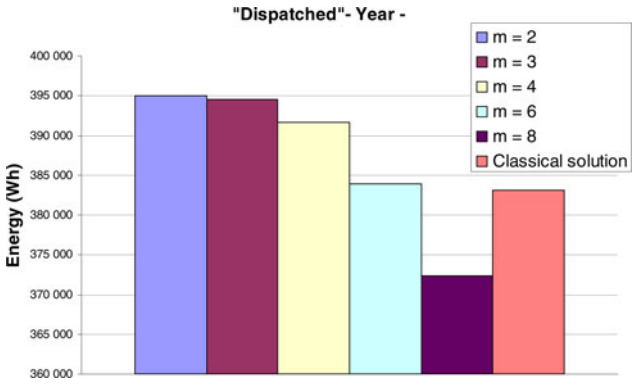

Fig. 13. Yearly energy produced (dispatched shaded cells).

When the shaded PV cells are grouped, the topology with two boosts is the most efficient.

The topologies with two, three, and four boosts have a similar annual energy production. These topologies produce nearly 10% more energy than the classical solution.

The topologies with six and eight boosts are less efficient than topologies with two, three, and four boosts, but they remain more efficient than the classical solution.

When the shaded PV cells are dispatched, the results are similar to the previous case but the levels of energy produced are smaller. The topologies with two, three, and four boosts clearly remain more efficient than the classical topology. The topology with two boosts remains the most efficient. On the other hand, the topologies with six or eight boosts have inferior or similar performances to the classical solution.

Output energies of different topologies drop with the number of boosts. This evolution follows the same curve of the output power found during the optimization, so these two results are coherent.

The study with a typical shadow confirms that the topology with two boosts is the most efficient.

X. Effect of an Important Mismatch

Previous studies have shown that the topology with two boosts is the most efficient. To confirm the interest of this topology compared with the classical solution, a study with an important heterogeneous irradiation on the PV field has been carried out.

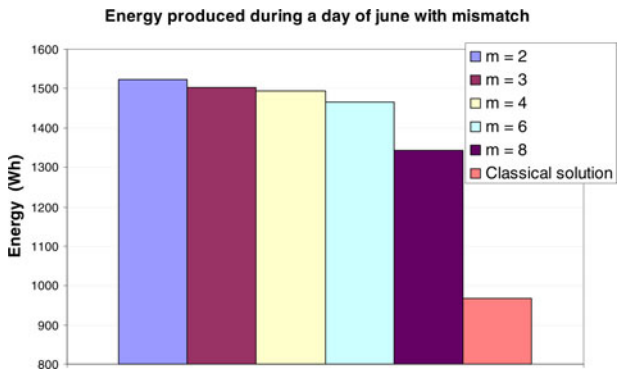

Fig. 14. Energy produces during a day of June with a mismatch.

To make this heterogeneous irradiation, a different level of irradiation has been applied to PV cells. The distribution of the solar irradiation (Irr in $\mathrm{W{\cdot}m^{-2}}$) on PV cells has the following pattern:

1) 75% of PV cells receive 100% of $\mathrm{Irr_{typ}}$, i.e., 108 cells receive 1000 $\mathrm{W{\cdot}m^{-2}}$;
2) 15% of PV cells receive 50% of $\mathrm{Irr_{typ}}$, i.e., 22 cells receive 500 $\mathrm{W{\cdot}m^{-2}}$;
3) 5% of PV cells receive 25% of $\mathrm{Irr_{typ}}$, i.e., 7 cells receive 250 $\mathrm{W{\cdot}m^{-2}}$;
4) 5% of PV cells receive 0% of $\mathrm{Irr_{typ}}$, i.e., 7 cells receive 0 $\mathrm{W{\cdot}m^{-2}}$.

These heterogeneous irradiation levels simulate the conditions in an urban context on a building integrated installation. In these installations, PV panels can have different orientations and inclinations, different levels of soiling, and some punctual soiling (droppings, leafs, etc.) [33].

The first comparison was been done on a day in summer (see Fig. 14). Under these conditions, the topology with two boosts is able to produce 1523 Wh while the classical solution produces only 963 Wh. The increase of the produced energy with the proposed topology is close to 60%.

The second comparison was been done on a day in winter. Under these conditions, the topology with two boosts is able to produce 369 Wh when the classical solution produces only 261 Wh. The increase of the produced energy with the proposed topology is 40%.

These simulations have shown that in a hard environment (building integrated installations) the topology with two boosts is able to produce much more energy than the classical solution.

XI. Conclusion

An optimization of a cascaded dc/dc converter devoted to grid-connected PV system has been proposed. This converter is based on a boost chopper circuit.

The correct operation and the advantages and the limits of this circuit have been checked by simulations on PSIM software.

Models of losses and volume of the boost have been developed to realize the optimizations.

However, the optimum depends on different parameters. To respond to these different variations, a flexible converter has been realized and tested. The experimental results confirm the extreme modularity and the good efficiency of this converter.

A particular study for a PV generator of 144 cells has been done. Under these conditions, the best solution is a topology with two boosts and with 72 PV cells per boost. The study of the shadow effects on these topologies confirms these results. This optimum topology (with two boosts) is also the most efficient when the PV field is shaded. In a typical case (shadow of a chimney), it is able to produce 4% extra energy. The increase of the produced energy can reach up to 60% of the classical solution in the case of an important irradiation mismatch on the PV field.

The properties of the PV field distributed topology are very interesting when the PV power generation systems have a partial shadowing issue. This distributed converter topology can strongly reduce the drawbacks related to building integrated PV systems.

REFERENCES

[1] W. Hoffmann, "PV on the way from a few lead markets to a world market," in *Proc. IEEE 4th World Conf. Photovoltaic Energy Convers.*, May 2006, vol. 2, pp. 2454–2456.

[2] J. M. Carrasco, L. G. Franquelo, J. T. Bialasiewicz, E. Galvan, R. C. P. Guisado, Ma. A. M. Prats, J. I. Leon, and N. Moreno-Alfonso, "Power electronics systems for the grid integration of renewable energy source—A survey," *IEEE Trans. Ind. Electron.*, vol. 53, no. 4, pp. 1002–1016, Aug. 2006.

[3] M. Bachler, "Grid connected systems in Europe—Looking into the future," in *Proc. IEEE 4th World Conf. Photovoltaic Energy Convers.*, May 2006, vol. 2, pp. 2289–2292.

[4] S. Liu and R. A. Dougal, "Dynamic multiphysics models for solar array," *IEEE Trans. Ind. Electron*, vol. 17, no. 2, pp. 285–294, Jun. 2002.

[5] G. Petronea, G. Spagnuoloa, and M. Vitelli, "Analytical model of mismatched photovoltaic fields by means of Lambert W-function," *Solar Energy Mater. Solar Cells*, vol. 91, pp. 1652–1657, 2007.

[6] R. H. Bonn, "Developing a 'next generation' PV inverter," in *Proc. IEEE Photovoltaic Spec. Conf.*, May 2002, pp. 1352–1355.

[7] G. Petrone, G. Spagnuolo, R. Teodorescu, M. Veerachary, and M. Vitelli, "Reliability issues in photovoltaic power processing systems," *IEEE Trans. Ind. Electron*, vol. 55, no. 7, pp. 2569–2580, Jul. 2008.

[8] D. R. Neill and B.S.M. Granborg, "Report on the photovoltaic R&D program in Hawaii," *IEEE Trans. Energy Convers.*, vol. EC-1, no. 4, pp. 43–49, Dec. 1986.

[9] S. Rahman and M. Bouzguenda, "A model to determine the degree of penetration and energy cost of large scale utility interactive photovoltaic systems," *IEEE Trans. Energy Convers*, vol. 9, no. 2, pp. 224–230, Jun. 1994.

[10] G. R. Walker and P. C. Sernia, "Cascaded DC–DC converter connection of photovoltaic modules," *IEEE Trans. Power Electron.*, vol. 19, no. 4, pp. 1130–1139, Jul. 2004.

[11] S. Cuk, "Basics of switched mode power conversion: Topologies, magnetics and control," in *Proc. IEEE Ind. Electron. Soc.*, 1991, pp. 265–269.

[12] A. Bratcu, I. Munteanu, S. Bacha, D. Picault, and B. Raison, "Power optimization strategy for cascaded DC–DC converter topologies of photovoltaic modules," presented at the IEEE International Conference on Industrial Technology, Gippsland, VIC, Australia, Feb. 2009.

[13] Y. Tsuchiya, "A photovoltaic AC fusion converter," *IEEE Trans. Energy Convers.*, vol. 14, no. 3, pp. 849–854, Sep. 1999.

[14] A. Ch. Kyritsis, E. C. Tatakis, and N. P. Papanikolaou, "Optimum design of the current-source flyback inverter for decentralized grid-connected photovoltaic system," *IEEE Trans. Energy Convers.*, vol. 23, no. 1, pp. 281–293, Mar. 2008.

[15] B. Yang, W. Li, Y. Zhao, and X. He, "Design and analysis of a grid-connected photovoltaic power system," *IEEE Trans. Power Electron.*, vol. 25, no. 4, pp. 992–1000, Apr. 2010.

[16] S. Vighetti, "Systèmes photovoltaïques raccordés au réseau: Choix et dimensionnement des étages de conversion," Ph.D. dissertation, G2Elab, Grenoble Univ., Grenoble, France, 2010.

[17] G. Lefèvre, "Conception de convertisseurs statiques pour l'utilisation de la Pile à Combustible," Ph.D. dissertation, LEG, Grenoble Univ., Grenoble, France, 2004.

[18] G. Lefèvre, H. Chazal, J-P. Ferrieux, and J. Roudet, "Application of Dowell method for nanocrystalline toroid high frequency transformers," presented at the IEEE Power Electronics Specialists Conference, Aachen, Germany, 2004.

[19] G. Lefèvre, J.-P. Ferrieux, J. Barbaroux, Ph. Boggetto, and P. Charlat, "Minimizing magnetic components losses in a new DC–DC converter for portable fuel cell applications," presented at the IEEE Industry Applications Society Conference, Seattle, WA, 2004.

[20] M. C. Costa and J.-L. Coulomb, "An object-oriented optimization library for finite element method software," *IEEE Trans. Magn.*, vol. 36, no. 4, pp. 1057–1060, Jul. 2000.

[21] J. M. A. Myrzik and M. Calais, "String and module integrated inverters for single-phase grid connected photovoltaic systems—A review," presented at the IEEE Power Tech Conference, Bologna, Italy, Jun. 2003.

[22] B. Delinchant, L. Estrabaut, L. Gerbaud, H. Nguyen Huu, B. Du Peloux, H.L. Rakotoarison, F. Verdiere, and F. Wurtz, "An optimizer using the software component paradigm for the optimization of engineering systems," *Int. J. Comput. Math. Electr. Electron. Eng.*, vol. 26, no. 2, pp. 368–379, 2007.

[23] G. Yilei, H. Lijun, and L. Zhengyu, "A flexible converter with two selectable topologies," *IEEE Trans. Ind. Electron.*, vol. 56, no. 12, pp. 4465–4472, Dec. 2009.

[24] J.-S. Lai, B. M. Song, R. Zhou, A. R. Hefner, D. W. Berning, and C. C. Shen, "Characteristics and utilization of a new class of low on-resistance MOS-gated power device," in *Proc. IEEE Ind. Appl. Soc. Conf.*, Oct. 1999, vol. 2, pp. 1073–1079.

[25] A. Elasser, M. Kheraluwala, M. Ghezzo, R. L. Steigerwald, N. A. Evers, J. Kretchmer, and T. P. Chow, "A comparative evaluation of new silicon carbide diodes and state-of-art silicon diodes for power electronics applications," in *Proc. IEEE Ind. Appl. Soc. Conf.*, Oct. 1999, vol. 1, pp. 341–345.

[26] W. Xiao and G. Dunford, "Modified adaptive hill climbing MPPT method for photovoltaic power systems," in *Proc. IEEE Power Electron. Spec. Conf.*, 2004, vol. 3, pp. 1957–1963.

[27] F.-S. Pai and R.-M. Chao, "A new algorithm to photovoltaic power point tracking problems with quadratic maximization," *IEEE Trans. Energy Convers*, vol. 25, no. 1, pp. 262–264, Mar. 2010.

[28] L. Fangrui, D. Shanxu, L. Fei, L. Bangyin, and K. Yong, "A variable step size INC MPPT method for PV systems," *IEEE Trans. Ind. Electron.*, vol. 55, no. 7, pp. 2622–2626, Jul. 2008.

[29] N. Femia, G. Petrone, G. Spagnuolo, and M. Vitelli, "A technique for improving P&O MPPT performances of double-stage grid-connected photovoltaic systems," *IEEE Trans. Ind. Electron.*, vol. 56, no. 11, pp. 4473–4481, Nov. 2009.

[30] T. Shimizu, M. Hirakata, T. Kamezawa, and H. Watanabe, "Generation control circuit for PV module," *IEEE Trans. Power Electron.*, vol. 16, no. 3, pp. 293–300, May 2001.

[31] S. Kobayashi, T. Iino, H. Kobayashi, K. Yamada, and T. Yachi, "Degradation of output characteristics of a small photovoltaic module due to dirt spots," in *Proc. 27th Int. Telecommun. Conf.*, Sep. 2005, pp. 435–439.

[32] European Commission, Joint Research Centre—Photovoltaic Geographical Information System (PVGIS)—PV estimation utility, [Online]. Available: http://re.jrc.europa.eu/pvgis/apps4/pvest.php

[33] A. Hunter Fanney, B. P. Dougherty, and M. W. Davis, "Performance and characterization of building integrated photovoltaic panels," in *Proc. IEEE Photovoltaic Spec. Conf.*, May 2002, pp. 1493–1496.

[34] P. G. Barbosa, H. A. C. Braga, Md. C. B. Rodrigues, and E. C. Teixeir, "Boost current multilevel inverter and its application on single-phase grid-connected photovoltaic systems," *IEEE Trans. Power Electron.*, vol. 21, no. 4, pp. 1116–1124, Jul. 2006.

[35] T. Shimizu, O. Hashimoto, and G. Kimura, "A novel high-performance utility-interactive photovoltaic inverter system," *IEEE Trans. Power Electron.*, vol. 18, no. 2, pp. 704–711, Mar. 2003.

[36] T. Shimizu, K. Wada, and N. Nakamura, "Flyback-type single-phase utility interactive inverter with power pulsation decoupling on the DC input for an

AC photovoltaic module system," *IEEE Trans. Power Electron.*, vol. 21, no. 5, pp. 1264–1272, Sep. 2006.

[37] A. Koran, K. Sano, R.-Y. Kim, and J.-S. Lai, "Design of a photovoltaic simulator with a novel reference signal generator and two-stage LC output filter," *IEEE Trans. Power Electron.*, vol. 25, no. 5, pp. 1331–1338, May 2010.

[38] M. G. Villalva, J. R. Gazoli, and E. R. Filho, "Comprehensive approach to modeling and simulation of photovoltaic arrays," *IEEE Trans. Power Electron.*, vol. 24, no. 5, pp. 1198–1208, May 2009.

Stéphane Vighetti was born in 1984. He received the Graduate degree in electrical engineering from the Grenoble Institute of Technology, Grenoble, France, in 2007, and the Ph.D. degree from Grenoble Electrical Engineering Laboratory (G2Elab), University Joseph Fourier, Grenoble, in 2010.

His current research interests include power electronics and photovoltaic systems.

Jean-Paul Ferrieux was born in 1959. He received the Ph.D. degree and the HDR, both in electrical engineering, from the Grenoble Institute of Technology, Grenoble, France, in 1984 and 1989, respectively.

He is a Professor at the University Joseph Fourier, Institut Universitaire de Technologie 1 (IUT1), Grenoble. His research activities take place at the Grenoble Electrical Engineering Laboratory (G2Elab), where he is the Leader of the Power Electronics research group. His research interest includes power electronics (static converter and resonant converter, integration). He has published more than 100 technical papers in these areas and is the coauthor of a power electronics book entitled *Switch-Mode Power Supplies, Resonant Converters*. (Dunod Publisher, Paris, 2006).

Yves Lembeye was in born 1966. He received the Ph.D. degree in electrical engineering from the Grenoble Institute of Technology, France, in 1997 and the HDR from Joseph Fourier University, Grenoble, in 2008.

He is currently a Professor at the University Joseph Fourier Institut Universitaire de Technologie 1 (IUT1), Grenoble, where he is involved in research activities at Grenoble Electrical Engineering Laboratory (G2Elab). His current research interests include low-power dc–dc and ac–dc converters, high-current low-voltage converters, and passive components integration.